



Original Paper

Combined use of fly ash and silica to prevent the long-term strength retrogression of oil well cement set and cured at HPHT conditions



Guo-Dong Cheng^a, Xue-Yu Pang^{a, b, *}, Jin-Sheng Sun^{a, b}, Zheng-Song Qiu^{a, b},
Chuang-Chuang Wang^a, Jian-Kun Qin^a, Ning Li^c

^a School of Petroleum Engineering, China University of Petroleum (East China), Qingdao, 266580, Shandong, China

^b National Key Laboratory of Deep Oil and Gas, China University of Petroleum (East China), Qingdao, 266580, Shandong, China

^c Oil and Gas Engineering Research Institute (Tarim Oilfield Company), China National Petroleum Corporation, Tarim, 841000, Xinjiang, China

ARTICLE INFO

Article history:

Received 2 November 2022

Received in revised form

8 May 2023

Accepted 12 September 2023

Available online 18 September 2023

Edited by Jia-Jia Fei

Keywords:

Fly ash

Long-term strength retrogression

High temperature

Quantitative X-ray diffraction (QXRD)

Partial or no known crystal structure

(PONKCS)

ABSTRACT

The long-term strength retrogression of silica-enriched oil well cement poses a significant threat to wellbore integrity in deep and ultra-deep wells, which is a major obstacle for deep petroleum and geothermal energy development. Previous attempts to address this problem have been unsatisfactory because they can only reduce the strength decline rate. This study presents a new solution to this problem by incorporating fly ash to the traditional silica-cement systems. The influences of fly ash and silica on the strength retrogression behavior of oil well cement systems directly set and cured under the condition of 200 °C and 50 MPa are investigated. Test results indicate that the slurries containing only silica or fly ash experience severe strength retrogression from 2 to 30 d curing, while the slurries containing both fly ash and silica experience strength enhancement from 2 to 90 d. The strength test results are corroborated by further evidences from permeability tests as well as microstructure analysis of set cement. Composition of set cement evaluated by quantitative X-ray diffraction analyses with partial or no known crystal structure (PONKCS) method and thermogravimetry analyses revealed that the conversion of amorphous C-(A)-S-H to crystalline phases is the primary cause of long-term strength retrogression. The addition of fly ash can reduce the initial amount of C-(A)-S-H in the set cement, and its combined use with silica can prevent the crystallization of C-(A)-S-H, which is believed to be the working mechanism of this new admixture in improving long-term strength stability of oil well cement systems.

© 2023 The Authors. Publishing services by Elsevier B.V. on behalf of KeAi Communications Co. Ltd. This is an open access article under the CC BY-NC-ND license (<http://creativecommons.org/licenses/by-nc-nd/4.0/>).

1. Introduction

Drilling and completion of deep and ultra-deep wells is a critical step of extracting petroleum and geothermal energies buried deep down the earth surface (Allahviridizadeh, 2020). Wellbore sealing integrity provided primarily by oil well cement is critical to safeguard stable production of these wells. The high temperature environment in deep and ultra-deep wells resulting in strength retrogression of oil well cement is a major cause of its wellbore integrity failure (Salim and Amani, 2013). As a commonly used cementitious material in well cementing, neat oil well cement systems experience significant strength declines when they are

cured at temperatures above approximately 110 °C (Krakowiak et al., 2015), which is caused by the change of hydration products from amorphous C-S-H to high calcium crystalline hydration products. A generally accepted practice to prevent the strength retrogression of oil well cement is adding silica powder to change hydration products into tobermorite and xonotlite with relatively good properties (Swayze, 1954). This approach seems to be effective for cement set at low temperatures before high temperature curing (Costa et al., 2017; Iverson et al., 2014; Jiang et al., 2021; Krakowiak et al., 2018; Pernites and Santra, 2016), which is applicable for simulating the upper wellbore sections in deep wells and steam-injection wells (Liu et al., 2021). However, several of our recent studies have revealed that silica-enriched oil well cement systems can experience severe long-term strength decline under simulated high-temperature deep-well conditions at 200 °C and 50–150 MPa (Li et al., 2020; Liu et al., 2022; Pang et al., 2021; Qin et al., 2023). The key difference between our study and most previous studies is

* Corresponding author. School of Petroleum Engineering, China University of Petroleum (East China), Qingdao, 266580, Shandong, China.

E-mail address: x.pang@upc.edu.cn (X.-Y. Pang).

the setting temperature (defined as the temperature at which liquid cement transforms to solid cement): our study employed a high setting temperature while most previous studies employed a low setting temperature before high-temperature curing. In order to address the newly discovered long-term strength retrogression issue of silica-enriched oil well cement systems, various influencing factors have been studied. The optimization of silica-based admixtures, including particle size, dosage and crystallinity may change the rate of strength decline, but cannot prevent the trend of microstructure coarsening and physical-mechanical property deterioration (Qin et al., 2023). Similarly, increasing curing pressure and adding physical reinforcement materials (such as nanographene and latex fiber) can slow down but not prevent the strength retrogression process (Liu et al., 2022; Qin et al., 2023). With the fast increase in the number of deep and ultra-deep wells being drilled worldwide (Hu et al., 2013; Pu et al., 2022; Wang et al., 2017), it is highly critical to find a proper solution to the long-term strength retrogression problem of oil well cement set and cured under high-temperature and high-pressure conditions.

The gradual formation of xonotlite from either amorphous C-S-H or tobermorite over long-term curing seems to be one of the primary causes of strength retrogression of silica-enriched oil well cement systems (Pang et al., 2021). Such transformation can cause volumetric shrinkage and microstructure coarsening because xonotlite has less bound water and a much higher density (Churakov and Mandaliev, 2008; Helmi et al., 2016; Shen et al., 2019). Previous studies have shown that the incorporation of aluminum into the structure of C-S-H can effectively prevent the transformation of tobermorite to xonotlite by aluminum substitution into the tobermorite crystal lattice structure at high temperatures (>150 °C) (Chow and Kalousek, 1976; Shaw et al., 2000). However, adding alpha-alumina to silica-enriched oil well cement has been proven to be ineffective in preventing strength retrogression possibly due to the low reactivity of alpha-alumina (Qin et al., 2023). As a solid waste released from the coal burning process, fly ash contains more reactive alumina and is widely available around the world. It is currently widely used in both oil well cement and construction cement as a supplementary cementitious material to improve durability and other properties (Ahmaruzzaman, 2010; Cho et al., 2019; Hemalatha and Ramaswamy, 2017; Hemalatha and Sasmal, 2019; Juenger and Siddique, 2015; Meng et al., 2017; Wang et al., 2019; Yildirim and Sümer, 2013). Fly ash has also been used as a raw material to prepare geopolymer systems for cementing applications, but the geopolymer systems has yet to see a full-scale implementation in oil and gas well cementing, especially in the cementing of ultra-deep wells and other complex conditions involving ultra-high temperature and high-pressure, due to various factors such as lack of supporting processes and standards (Adjei et al., 2022; Ahdaya and Imqam, 2019; Khalifeh et al., 2018; Paiva et al., 2018; Salehi et al., 2019). During this study, the effectiveness of fly ash as a strength retrogression admixture used both individually and in combination with silica sand are investigated. Oil well cement systems containing fly ash are designed with sufficient amounts of retarder to meet deep-well cementing requirements and are directly exposed to HPHT curing condition of 200 °C and 50 MPa to simulate the conditions of deep wells and ultra-deep wells. The physical and mechanical property change of set cement are evaluated in both macroscopic and microscopic scales and monitored up to a curing period of 90 days.

Analyzing the phase composition change of set cement with curing time is critical for understanding the mechanism of strength retrogression. Quantitative X-ray diffraction (QXRD) analysis is a commonly used method for phase quantification of both anhydrous cement and hydrated cement (Christidis et al., 2021; Jansen et al.,

2012; Le Saoût et al., 2011; Mejdi et al., 2022; Polavaram and Garg, 2021; Scrivener et al., 2004; Soin et al., 2013; Wei et al., 2012; Wolf et al., 2019, 2020). However, because cement hydration products contain significant amounts of amorphous phase, either an internal or external standard is needed to perform QXRD analysis on hydrated cement. Additionally, since fly ash contains significant amounts of amorphous phases that may or may not be fully reacted during hydration, fly ash modified cement-based materials generally contain multiple different amorphous phases. The use of internal or external standard can help to determine the total amount of amorphous phase but not the individual contents of various amorphous phases. Scarlett and Madsen (2006) proposed a partial or no known crystal structure (PONKCS) method, which can be combined with the classic Rietveld refinement to calculate the content of the unknown or partially known phase (PONKCS phase). The diffraction pattern of the PONKCS phases (which can be either crystalline, amorphous or mixed phases) can be fitted by a Le Bail or Pawley model and treated as if it has a known crystal structure during Rietveld refinement. This method is widely used in many studies and is an important means to study cement systems containing mineral admixtures such as fly ash and granulated blast furnace slag (Bullerjahn and Mehringskötter, 2021; De Matos et al., 2022; Naber et al., 2019; Snellings et al., 2014; Stetsko et al., 2017; Sun and Vollpracht, 2018). During this study, Rietveld refinement is employed in combination with PONKCS method and external standard method to determine phase compositions of high-temperature oil well cement systems containing fly ash.

2. Materials and experimental methods

2.1. Materials

Class G oil well cement, 53 μm silica flour and chemical additives used in cement slurries were the same as those used in our previous studies (Pang et al., 2021; Qin et al., 2023). Four kinds of commercially available fly ash used in this study came from the same power plant in Shanxi, China. They were all class F fly ash according to ASTM C618. However, they present slight differences both in particle size distribution and composition. It is possible for fly ash from the same power plant to present differences in reactivity despite similar compositions (Wang et al., 2019). Fig. 1 and

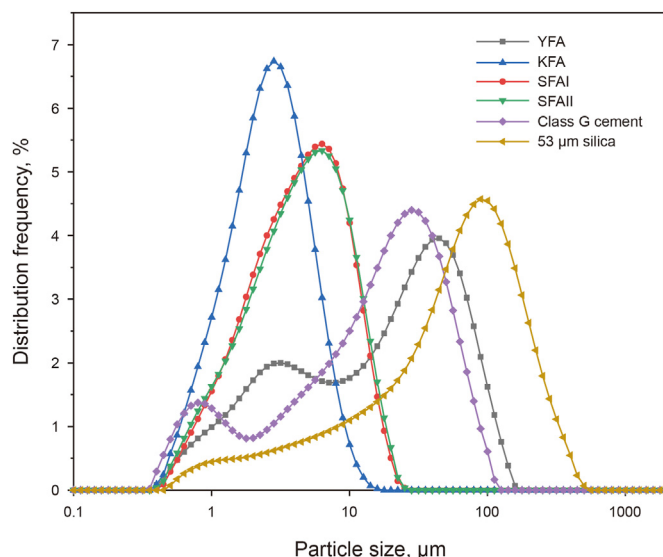


Fig. 1. Particle size distribution analysis of dry blend materials.

Table 1 provide the particle size distribution test results of the bulk materials used. Table 2 presents XRF oxide analysis results. Here, YFA is the original unground fly ash; KFA is a different product with much lower Al_2O_3 content and ground to much smaller sizes; SFAI has the same composition as YFA, but was ground to finer sizes, SFAII is a different batch of the same product as SFAI. It can be seen that SFAII contain higher amount of SiO_2 and lower amounts of minor oxide (such as Fe_2O_3 and CaO , etc.), compared to SFAI. X-ray powder diffraction revealed that the crystalline mineral in the four types of fly ash included quartz, anhydrite, mullite, and hematite, as shown in Fig. 2. The XRD diffractograms of all fly ashes showed the characteristic reflections of amorphous structure in the range of $25^\circ \sim 30^\circ$, while the 53 μm silica had mainly quartz with high crystallinity. The XRD diffractograms of class G cement and 53 μm silica can be found in our previous study (Pang et al., 2021).

2.2. Formulation design and slurry preparation

Table 3 presents the formulation design of the slurries tested during this study. Slurry C_0 was the control design with 70% silica flour; slurries m_1 to m_4 were designed with 60% fly ash and no silica flour; slurries M_1 to M_4 were designed with both fly ash and silica flour. The CaO/SiO_2 molar ratio in the blended systems (M_1 to M_4) was close to 0.83 in reference to the chemical formula of tobermorite. All slurries were designed with a final density of 1.9 g/cm^3 . The liquid additives used were the same as those in our previous studies (Pang et al., 2021; Qin et al., 2021). The dosages of dispersant, retarder, fluid loss additive and defoamer were 5.5%, 4.5%, 6% and 0.5% by weight of cement, respectively. The defoamer was a pure liquid, while the solid contents in other liquid additives were all 20%. Because most of the different fly ash products used in this study (YFA, SFAI and SFAII) have very similar compositions with only particle size and batch differences, the corresponding slurries m_1 , m_3 and m_4 (as well as slurries M_1 , M_3 and M_4) are not expected to exhibit significantly different performances, especially in the long-term. All slurries presented in Table 3 were produced for 2 d short-term curing; while only selected slurries were produced for long-term curing (slurries C_0 , m_2 , m_3 , M_2 and M_3 for 30 d, slurries M_1 , M_2 , M_3 and M_4 for 90 d). This is primarily due to equipment (HTHP autoclave) availability, considering that it is very time consuming to perform long-term curing; the selection of long-term testing slurries was based on short-term test results. In a previous study, we have demonstrated that our experimental protocols will generated highly reproducible results between different batches (Qin et al., 2021).

During this study, dry blend of cement mixture were added to mixing water and liquid additive in a laboratory blender at a speed of 600 rpm, followed by final mixing at a speed of 3000 rpm for 35 s. The reduced shear rate was employed to avoid causing density increase of the slurry, because small amounts of hollow particle (cenospheres) may be present in the fly ash. After mixing, the slurry was poured into stainless steels mold (25 mm \times 70 mm internal dimension) and directly put inside autoclaves for high temperature and high pressure (HTHP) curing at $200^\circ\text{C}/50 \text{ MPa}$.

Table 1

Summary of material properties: particle size, surface area and specific gravity.

Material	D10, μm	D50, μm	D90, μm	Surface area, m^2/kg	Specific gravity
YFA	1.58	18.05	67.37	492	2.90
KFA	0.94	2.47	5.55	1187	2.66
SFAI	1.24	4.19	10.51	816	2.64
SFAII	1.18	4.27	10.92	830	2.57
53 μm silica	4.04	53.0	163	234	2.67
Class G cement	0.96	14.33	45.03	524	3.25

Table 2

Main oxides of bulk materials used.

Oxide name	YFA	KFA	SFAI	SFAII	53 μm silica	Class G cement
Al_2O_3	38.695	26.589	39.465	39.585	1.033	2.985
CaO	3.788	5.649	3.330	2.055	1.452	65.134
Fe_2O_3	3.385	7.547	3.138	0.597	0.866	6.675
TiO_2	1.820	7.156	1.923	2.167	0.051	—
K_2O	0.621	1.294	0.985	0.531	0.260	0.805
MgO	0.397	0.163	0.855	0.023	0.399	1.962
Na_2O	0.097	—	0.138	—	0.190	0.179
SO_3	2.604	1.652	2.456	2.155	0.212	3.15
P_2O_5	0.271	2.005	0.274	0.154	0.023	0.043
SiO_2	47.994	46.111	47.057	52.548	95.412	18.452
Free lime	0.46	0.03	0.03	0.09	—	1.65

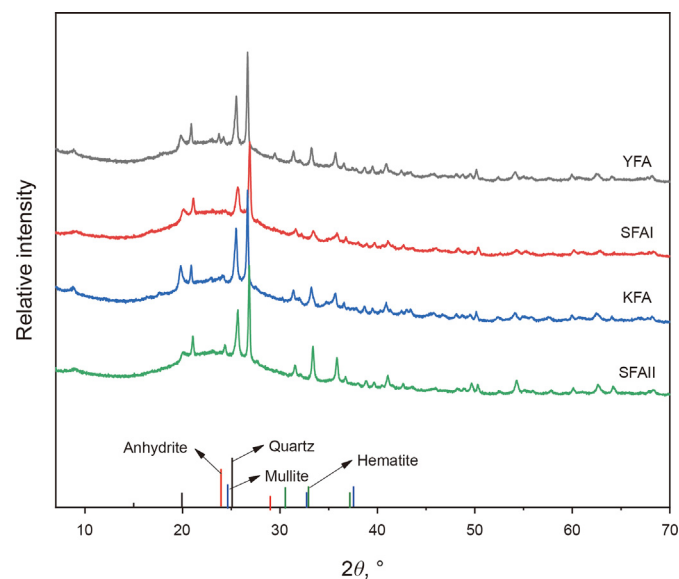


Fig. 2. Phase analysis of fly ash.

3. Test method

3.1. Macroscopic property analysis of set cement

Macroscopic properties of the cement studied include compressive strength and permeability. Compressive strength tests were performed using a UTM5105X load frame from Shenzhen SUNS Technology Company. Water and gas permeability tests were measured using test devices manufactured by Hai-An Hua Cheng Company according to GB/T 19139-2012 China national standard. Three replicate specimens were produced for each condition to obtain the average and variability of compressive strength in test result, while two replicate specimens in the same batch were used for water and gas permeability tests to obtain the average. More detailed information about these test methods can be found in our previous studies (Pang et al., 2021).

Table 3
Formulation design of dry blend compositions and added water.

Formulation	Cement	Fly ash	53 μm silica	Suspension aid	Added water	Initial porosity
C ₀	100	0	70	2.5	52.6	51.8
m ₁	100	60(YFA)	0	2.5	53.2	54.4
m ₂	100	60(KFA)	0	2.5	49.4	52.1
m ₃	100	60(SFAI)	0	2.5	48.9	51.8
m ₄	100	60(SFAII)	0	2.5	47.7	51.1
M ₁	100	60(YFA)	45	2.5	67.6	52.7
M ₂	100	60(KFA)	45	2.5	63.7	50.8
M ₃	100	60(SFAI)	33.8	2.5	59.7	50.9
M ₄	100	60(SFAII)	33.8	2.5	58.5	50.3

Note: the dry blend compositions and added water were all in % by weight of cement; the initial porosity equal to total liquid content in % by volume of cement slurry and included water in liquid additives.

3.2. Microscopic property analysis of set cement

Microstructure of set cement was studied by Scanning Electron Microscope (SEM) and Mercury Intrusion Porosimetry (MIP). A field emission SEM by JEOL (Model JSM-IT500LV) was used to obtain microstructure images. Sample preparation (epoxy impregnation and polishing) method was the same as that used in our previous study (Pang et al., 2021). The images were collected at a voltage of 15 kV and a current of 60 μA . A Quantachrome mercury intrusion pore size analyzer (model PM 33) was used to measure porosity and pore size distribution of the set cement. Small pieces of sample with largest dimension less than 5 mm and a total mass of approximately 1 g was used. The maximum pressure applied was 32,000 psi (220 MPa).

3.3. Set cement composition analysis

Cement composition was evaluated by Thermogravimetry (TG) and X-ray diffraction (XRD) analyses. TG tests were conducted using a Setaram thermal analysis instrument (Model Setline STA) with nitrogen as the protective gas. Temperature scheme include initial ramping from 28 to 105 $^{\circ}\text{C}$ at 5 $^{\circ}\text{C}/\text{min}$ and hold for 1 h, followed by final ramping from 105 to 1000 $^{\circ}\text{C}$ at 5 $^{\circ}\text{C}/\text{min}$. The sum of weight losses during all stages were considered as total water content of the sample for subsequent QXRD analysis. XRD data were collected using a Panalytical diffractometer (Model Aeris with a 600 W Cu-anode source, $\lambda = 1.541 \text{ \AA}$) operated at 40 kV and 15 mA. All scans were measured over an angular range of 7–70 $^{\circ}$ (2θ angle) with a 0.01 $^{\circ}$ 2θ step size and scanning time per step of 75.22 s, resulting in a total measurement time of about 30 min per scan.

Rietveld refinement analysis was carried out using Highscore Plus 5.0 software with International Diffraction Center Database (ICDD) and Crystallography Open Database (COD) to assess the quantities of main crystal phases as well as the amorphous phase. Similar to our previous study (Pang et al., 2022), a single crystal silicon was ground into fine powders and used as an external standard. The following equation was used to calculate the phase content of a sample (Scrivener et al., 2016):

$$W_j = \frac{S_j \rho_j V_j^2}{S_s \rho_s V_s^2} W_s \frac{u_m}{u_s} \quad (1)$$

where W_j is the weight fraction of phase j in the sample, S_j is the scale factor obtained in the Rietveld refinement for phase j , ρ_j is the unit cell density of phase j , V_j designates the unit cell volume of phase j ; similarly, S_s , ρ_s , and V_s represent the corresponding parameters of the standard material; W_s is the weight fraction of the standard phase in the external standard material (100% in our study); u_m and u_s are the mass absorption coefficients (MAC) of the

sample and the standard material, respectively. The calculation of MAC requires the oxide composition and total water content (obtained by TG tests) in a sample.

4. Test results and discussion

4.1. Compressive strength

Fig. 3 summarizes the compressive strength test results of cured slurries at various curing time. The compressive strength of the control slurry C₀ decreased from 63.18 to 8.95 MPa from 2 to 30 d curing time, suggesting that the traditional silica-enriched system experienced severe strength retrogression (86% decline) in the 30 d curing period, confirming our recent study (Pang et al., 2021). The decline rate was significantly faster than previously investigated systems at the same test condition, possibly due to larger silica particle sizes and different dosages of additives (Pang et al., 2021; Qin et al., 2023). Numerous studies showed that fly ash-cement blend systems typically had lower early strength at lower curing temperatures (Giergiczny, 2019; Lam et al., 2000; Li et al., 2021; Ma et al., 2016). Similarly, the use of fly ash instead of silica as admixture severely decreased the 2-day strength of the set cement (by about 50%) at HPHT conditions and cannot prevent the long-term strength retrogression of oil well cement systems in the 30 d curing period. The compressive strength of slurries m₂ and m₃ declined by 48.27% and 60.71%, respectively, from 2 to 30 d curing. However, the combined use of fly ash and silica appeared to have effectively halted the severe strength decline of oil well cement. Slurries M₁ through M₄ exhibited stable or increased strength during long-term curing up to 90 d. With curing time increased from 2 to 90 d, the compressive strength of slurry M₂ was little changed, while the compressive strengths of slurries M₁, M₃ and M₄ increased 33.0%–101%. The slight decrease (21%) in compressive strength of slurry M₂ from 2 to 30 d may be due to natural experimental uncertainties as compressive strength test results of cement can be subjected to the influences of multiple factors. The improved long-term strength of cement-silica-fly-ash systems (M systems) may be related to the favorable change of hydration products and would be explained in the following XRD analysis section. It was worth pointing out that there were no significant differences among the 90 d test results of slurries M₁, M₂, M₃, and M₄, suggesting that the properties of fly ash just affected early strength and had relatively little influence on the long-term performance of the blended systems, in agreement with other studies at lower temperatures (Antiohos et al., 2007; Cho et al., 2019; De Maeijer et al., 2020; Ma et al., 2016).

4.2. Water and gas permeability

As oil well cements are typically at water saturated state under

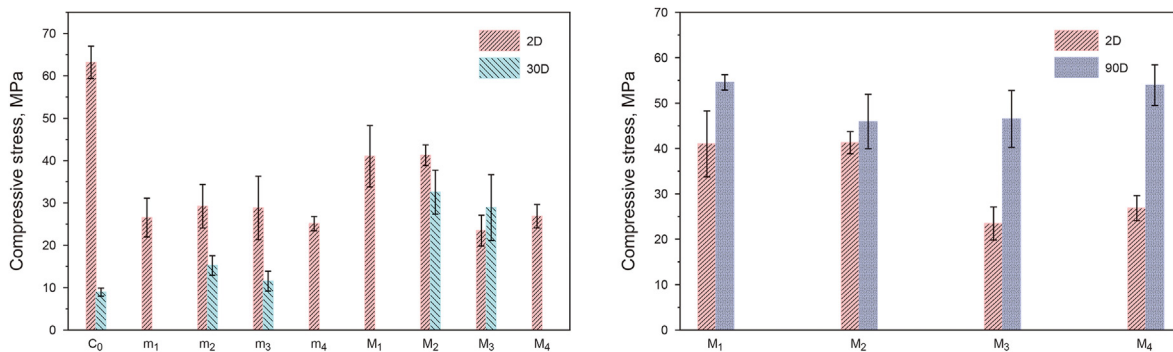


Fig. 3. Compressive strength test results of cured slurries at various curing time.

downhole condition due to the presence of formation fluids, water permeability is a more relevant parameter to evaluate their zonal isolation effectiveness. Water and gas (Klinkenberg) permeability test results of different slurries are displayed in Fig. 4. Gas permeability test was only conducted on selected slurries because it requires an extra drying process and does not reflect the true service condition. The test results indicated that the water permeability of the control slurry C_0 increased by nearly one order of magnitude from 2 to 30 d curing, i.e. from 0.0038 to 0.0212 mD. Although the 2-day compressive strengths of the fly ash slurries (m_1 to m_4) were only about 50% of that of the control, these slurries seem to have comparable water permeability as the control. This is due to

differences in hydration products and microstructure that will be further discussed later. Consistent with compressive strength test results, the use of fly ash alone was not able to prevent permeability increase of the set cement with increasing curing time, while the combined use of silica and fly ash can completely reverse such trend of permeability change. The water permeability of slurry M_3 was reduced by nearly one order of magnitude from 2 to 90 d (total reduction approximately 79.7%). The water permeability of slurries M_1 , M_2 and M_4 was also reduced by 59.8%, 36.2% and 65.5%, respectively. Set cement is known to have significantly higher gas permeability than water permeability due to coarsening of C-S-H structure during drying (Pang et al., 2021; Zhou et al., 2017). Test

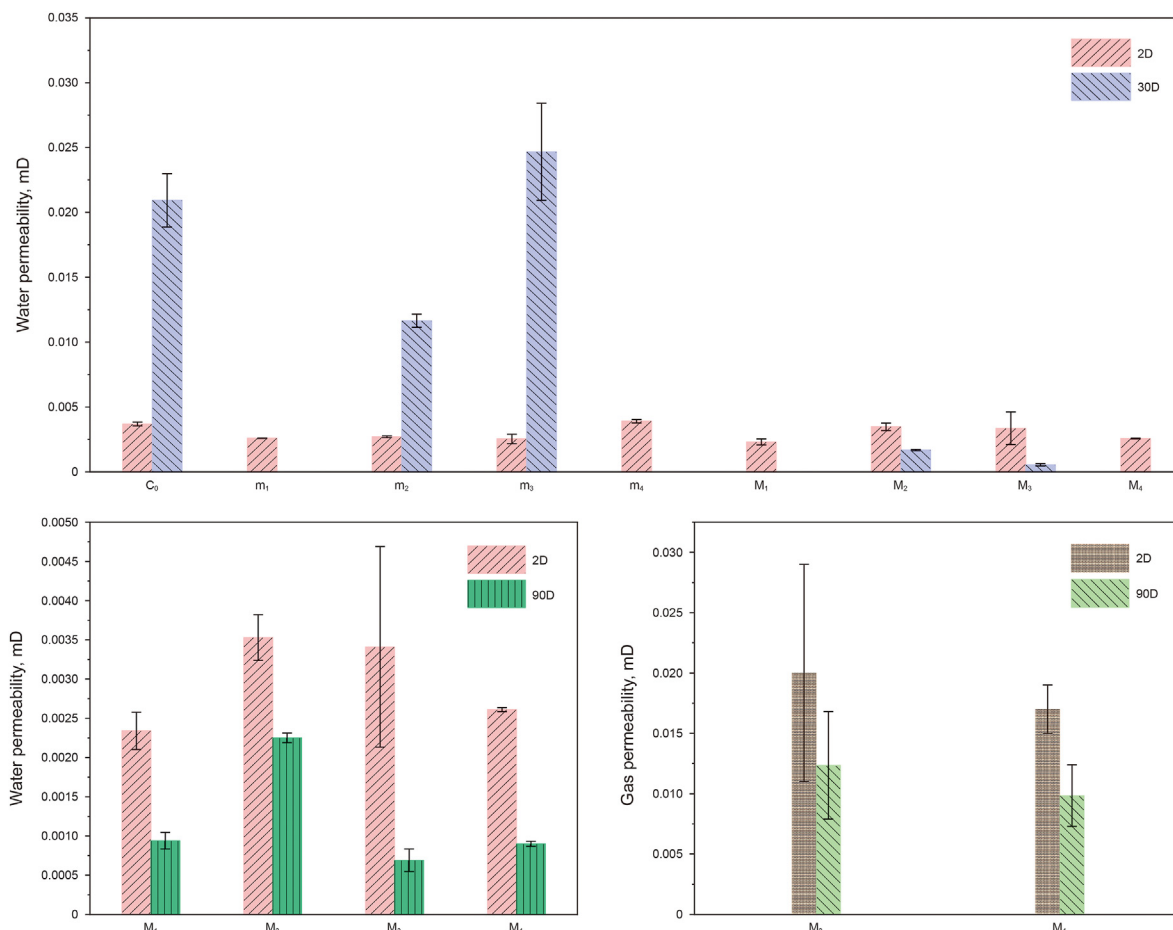


Fig. 4. Water permeability and gas permeability test results of set cement at various curing time.

results of slurries M_2 and M_3 indicate that gas permeability was decreased along with water permeability. They also confirmed previous findings that gas permeability were significantly higher than water permeability. It is clear from the test results of this study that the combined addition of fly ash and silica flour can effectively prevent permeability increase of oil well cement systems over long-term curing at HPHT conditions. The reduction in permeability is related to the favorable change of hydration products and would be explained in the following XRD analysis section.

4.3. MIP analysis

Fig. 5 displays the mercury intrusion test results of selected specimens. According to the aperture division principle proposed by Guo et al. (2016) and Shen et al. (2018), the pore structure of cement-based materials can be generally divided into four types: harmless pores (< 20 nm), less harmful pores (20–50 nm), harmful pores (50–200 nm) and more harmful pores (> 200 nm). This division principle was originally proposed based on the impact of pores on the tensile strength of cement-based materials during free-thaw actions, which is further employed here for pore size classifications. During 2–30 d curing, the total porosity increased from 25.3% to 38.0% in the control slurry C_0 , where the pores larger than 50 nm increased from 8.7% to 26.5%. In all samples containing both fly ash and silica, the pores larger than 50 nm showed a decreasing trend with time, while the pores less than 50 nm remained stable or increased slightly. This is in great contrast to oil well cement systems containing only silica as anti-strength retrogression additive (Pang et al., 2021). Overall, the total porosity of all samples containing both fly ash and silica varied slightly from 33.9% to 35.9%. The total porosities of slurries M_1 , M_2 and M_4 showed slight reductions with time, which was primarily attributed to the volume reductions of larger pores. The total porosity of slurry M_2 remain almost constant with time, but the proportion of small pores slightly increased. All slurries containing both fly ash and silica exhibited similar total porosities and pore size distributions after 90 d curing. Therefore, all test results, including compressive strength, permeability, and porosity analysis, appeared to show that the types of fly ash used had no significant differences in their abilities to prevent the long-term deteriorations of set cement properties at HPHT conditions. It can be concluded that the slurries containing both fly ash and silica exhibited stable microstructure and macroscopic properties over the 90 d curing period evaluated, with no retrogression behavior observed.

Additionally, during long-term curing from 2 to 30 d, the span and median of pore size of control slurry C_0 significantly increased with curing time increasing: the span increased from approximately 7–400 nm to 7–1000 nm and the median increased from 30 to 100 nm, indicating that it apparently experienced microstructure coarsening with increasing curing time. The pore size of slurries containing both fly ash and silica (M_1 to M_4) at all curing ages spans from about 7 to 600 nm with a median of 30–60 nm, which reduced slightly with curing time increasing, indicating that the combined use of fly ash and silica effectively prevented microstructure coarsening of oil well cement systems over long-term curing at HPHT conditions, consistent with permeability test results. As shown from the derivative curves, most selected specimens exhibited two main distribution peaks: one located between 15 and 30 nm and the other located between 50 and 150 nm. During long-term curing, the pore sizes corresponding with both distribution peaks increased with time for slurry C_0 but decreased with time for slurries M_1 to M_4 . Backscattered electron images confirm the test results observed by MIP and were included in the appendix.

4.4. XRD analysis

XRD was used to identify the mineral compositions of set cement. It can be seen from Fig. 6 that the main hydration products of control slurry C_0 mainly included semi-crystalline C-S-H, tobermorite and xonotlite, while the addition of fly ash changed the hydration product of oil well cement system to include more alumina-bearing phases such as katoite, grossular and possibly some new semi-crystalline phases (including C-(A)-S-H) as reflected by broadened peaks ranging from 28.5° to 33.5° . During long-term curing from 2 to 30 d, the control slurry C_0 showed increasing crystallinity as reflected by the diminishing amorphous C-S-H peak between 28.5° and 30.5° and the sharpening of the crystalline peaks at 28.9° , which was the main cause for the strength retrogression of traditional system at HPHT conditions, confirming our recent study (Pang et al., 2021). The use of fly ash instead of silica as admixture significantly changed the initial mineral composition of the set cement at 2 d. For the slurries containing fly ash only (m_2 and m_3), significant increases in katoite and grossular peak intensities were observed with increasing curing time to 30 d. In contrast, the XRD diffractograms of the slurries containing both fly ash and silica (M_1 to M_4) seemed to be much more stabilized and changed relatively little with increasing curing time, which explained the admixture's effectiveness in preventing strength retrogression.

In order to further explore the working mechanism of fly ash in preventing the long-term decline of silica-enriched oil well cement systems set and cured at HPHT conditions, quantitative analysis of mineral composition was conducted for all systems. Using the PONKCS model of amorphous phase in fly ash to assess the reactivity of fly ash may be more accurate than using that of the bulk composition due to possible asynchronous reactions of different phases in fly ash (Sun and Vollpracht, 2018). Therefore, for the fly ash modified systems, quantitative analysis of the mineral composition was conducted by using the PONKCS model of amorphous phase in fly ash (hereafter referred to "FA-amor" model) in combination with the external standard method. The diffraction pattern of crystalline mineral components in fly ash was subtracted from that of the bulk composition to create PONKCS pseudo-structures for the amorphous phases in fly ash. The amorphous phases of fly ash were regarded as cubic structures with an $Fd\bar{3}m$ space group (space group No.227). The background was fitted using Chebyshev polynomial of the first kind. The total amount of amorphous phases in fly ash was first estimated by the internal standard method at a dosage of 20% standard material (rutile powder with 99.9% purity) and shown in Table 4. The "pseudo formula mass" can be determined to obtain the basic models of fly ash amorphous phase, which are given in Table 5 and Fig. 7. Detailed modeling process can be found in the literature (Stetsko et al., 2017). To verify the accuracy of these models, four kinds of fly ash were mixed with the standard material (rutile) at dosages of 20%, 40%, and 60%, respectively, and wet ground thoroughly in absolute ethanol for 10 min. The QXRD results obtained by using the FA-amor PONKCS model and external standard method was compared with the internal standard method in terms of the total amorphous phase content. The two estimations were very close to each other and the difference ranged from 2.43% to 4.97%, indicating that the constructed FA-amor models were reliable, as shown in Fig. 8. It was worth noting that the error got slightly larger as the dosage of the standard material increased from 20% to 60% (with amorphous phase content decreased), which could be attributed to the dramatic signal differences between diffraction peaks of rutile and fly ash (the highest peak of rutile was 14–24 times as high as that of fly ash).

In addition to the amorphous phase contained in fly ash, the hydrated cement also contains amorphous hydration products,

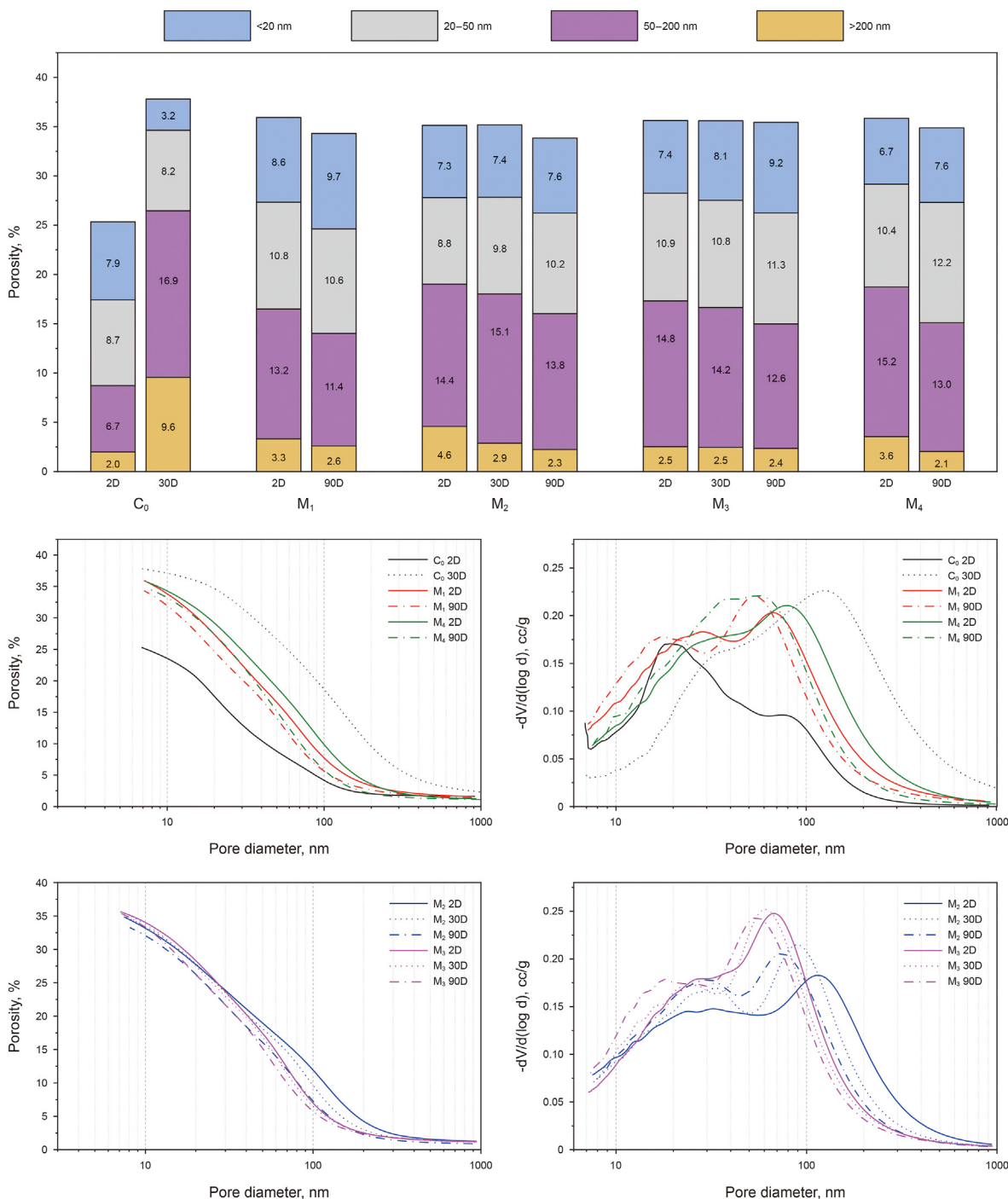


Fig. 5. MIP test results of selected specimens.

which mainly consists of C-(A)-S-H. Ideally, the weak diffraction pattern of C-(A)-S-H should be accounted for during the Rietveld refinement of the set-cement XRD profile. However, the C-S-H diffraction pattern obtained at low curing temperature, which worked well in XRD refinement of cement-silica systems (Qin et al., 2022), did not seem to fit well in the systems containing fly ash, possibly due to different structures. The contents of all unidentified amorphous phase (UAP) in hydrated cement were estimated by the external standard method described in Section 3.3. The content of C-(A)-S-H phase was assumed to be equal to that of UAP.

Here, all systems were classified into stable systems (M_1, M_2, M_3, M_4) and unstable systems (C_0, m_1, m_2, m_3, m_4). The samples of the

stable system were tested twice to check the repeatability of QXRD analysis results and the average standard deviation in measured phase content was approximately 0.37%. Representative refinement results of the diffractograms are presented in the appendix (Fig. A4 to Fig. A7). The refined phase contents of the unstable systems are presented in Fig. 9. The amorphous C-(A)-S-H is known to be one of the best phases contributing to the strength of set cement, while xonotlite is among one of the worse phases. The content of amorphous C-(A)-S-H was reduced with increasing curing time in the control slurry C_0 , as well as in slurries m_2 and m_3 , suggesting continuous crystallization of amorphous C-(A)-S-H in these systems, which was the main cause of strength retrogression.

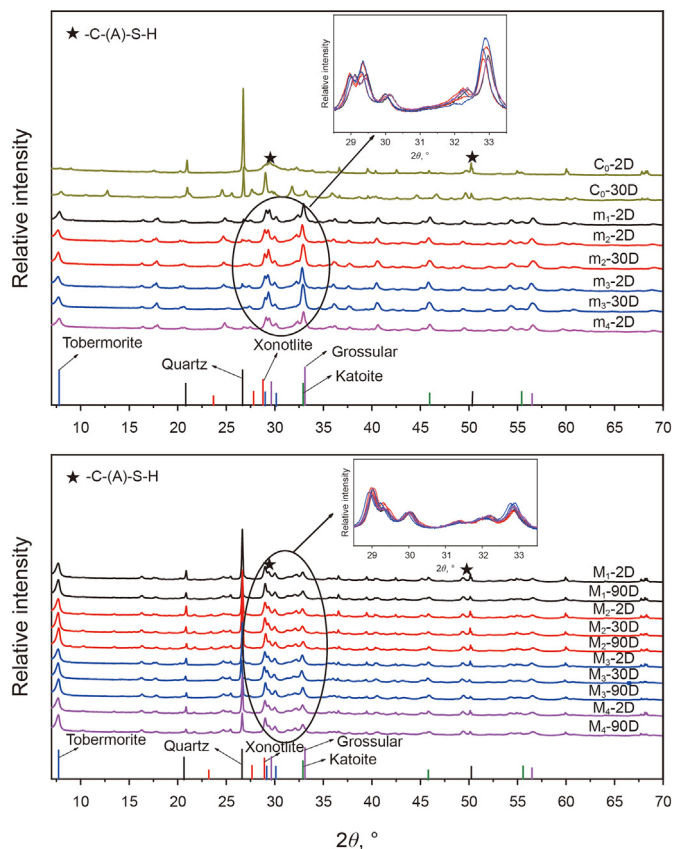


Fig. 6. X-ray diffraction analysis of set cement at various curing time.

Table 4
Phase analysis results for different fly ash by internal standard method.

Phase	YFA	KFA	SFAI	SFAII
Quartz	4.9	4.3	4.8	4.8
Hematite	2.0	1.2	2.8	3.1
Anhydrite	3.8	2.7	3.0	3.5
Mullite	0.3	0.8	0	0
Muscovite 2M1	2.2	2.4	1.6	1.9
Calcite	0.2	0	0	0
Amorphous	86.5	88.7	87.8	86.7
RWP	3.1328	2.9573	2.8546	2.7873

However, while the reduction of amorphous C-S-H in the control slurry C₀ was quite significant and accompanied mainly by the increase of tobermorite and xonotlite contents, the reduction of amorphous C-(A)-S-H in slurries m₂ and m₃ was relatively small and accompanied mainly by the increase of katoite content.

The refinement results of the stable systems are presented in Fig. 10. In contrast with the unstable systems, the contents of amorphous C-(A)-S-H in all the stable systems were increased with curing time increasing, suggesting that the amorphous C-(A)-S-H in these systems had excellent stability at such high temperature, which was the main reason that fly ash can prevent long-term

Table 5
Parameter of FA-amor models.

Parameter	YFA-amor	KFA-amor	SFAI-amor	SFAII-amor
Pseudo formula mass	9.5	2.4	10.7	10.1
Space group number	227	227	227	227
Side length of unite cell (a = b = c)	6.46	10.7	6.52	6.51
Caglioti W left	159.9	123.7	148.2	157.7

strength retrogression of silica-enriched oil well cement systems set and cured under HPHT conditions. The improvement of the physical and mechanical properties with increasing curing time observed in previous sections may also be attributed to the increasing C-(A)-S-H content in the set cement, mainly as a result of continued reaction of fly ash and silica. Additionally, all fly ash modified slurries contain significantly more tobermorite and less xonotlite than the control slurry, which further proved that the incorporation of aluminum into the structure of C-S-H can prevent the transformation of tobermorite to xonotlite by aluminum substitution into the tobermorite crystal lattice structure at high temperatures (>150 °C) (Chow and Kalousek, 1976; Shaw et al., 2000). It is believed that having more tobermorite in set cement is beneficial to long-term strength stability at high temperature owing to its dense fibrous microstructure (Reddy et al., 2016; Juge et al., 2008). It is worth noting that the addition of fly ash reduced the initial amorphous C-(A)-S-H content in all slurries after 2 d curing, which can explain their lower initial strength compared with the control slurry C₀. The long-term strengths of the cement-silica-fly-ash systems were much better than slurry C₀ at 30 d due to significantly less xonotlite phase generated. Finally, it should be stressed that mineral composition is not the only factor controlling cement strength, because the microstructure of the same mineral may be different depending on their condition of formation.

The composition evolution of different systems from the initial unhydrated state to the states at various curing time are presented in Fig. 11. Consistent with our previous studies (Qin et al., 2021, 2022), class G cement was found to have completely reacted at such high curing temperature after 2 d curing. In the cement-silica system (control slurry C₀), the percentage of quartz reacted increased from 50.8% to 75.1% from 2 to 30 d curing. In the cement-fly-ash systems, fly ash was almost completely consumed after 30 d curing (see slurries m₂ and m₃). The degree of reaction of fly ash was significantly reduced in the cement-silica-fly-ash systems (M systems) compared to that in the cement-fly-ash systems (m systems). This is probably because fly ash has to compete with silica to react with cement in the M systems, which is the fastest reacting phase. The amount of quartz and fly ash consumed in slurries M₁ to M₄ varied widely among different systems: The amount of quartz consumed in slurries M₃ and M₄ were 59.7% ± 1.6%, more than those consumed in slurries M₁ and M₂ (45.8% ± 0.3%), after 90 d curing. The amount of fly ash consumed in slurries M₃ and M₄ were also the highest, at approximately 64.4% after 90 d curing. Overall, it appears that large particle size (YFA in M₁) and lower Al₂O₃ content (KFA in M₂) significantly reduced the reaction rate of fly ash during the hydration process. Numerical data of Figs. 9–11 are included in the appendix (Tables A1 and A2).

4.5. TGA analysis

Fig. 12 present the TGA results of slurries at various curing time. At the age of 2 d, the non-evaporable water content of control slurry C₀ was about 0.13 g/g dry blend, which reduced to only 0.07 g/g dry blend after 30 d curing, suggesting that chemically combined water content was decreased due to conversion of hydration products from amorphous C-(A)-S-H to crystalline phases. The primary decomposition peak shifted from approximately 210 to 760 °C,

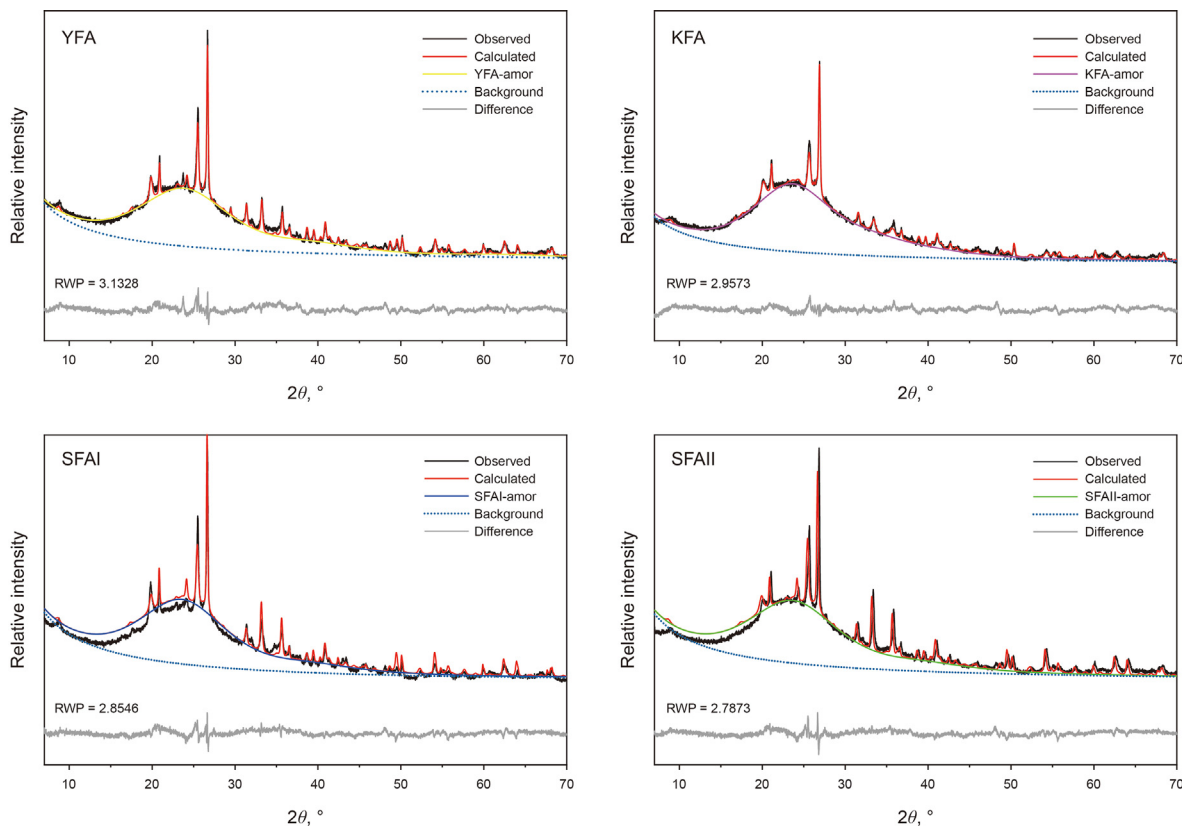


Fig. 7. Refinement of fly ash diffraction patterns and derivation of their amorphous phase models.

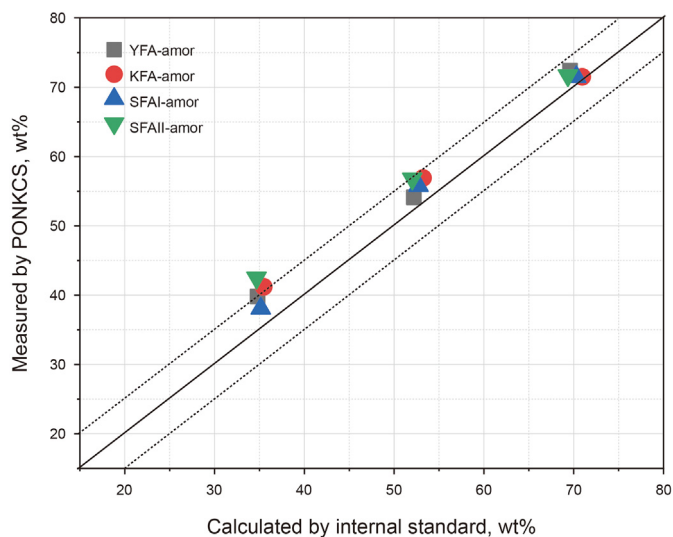


Fig. 8. Plot of the QXRD results of amorphous phase measured by POKKCS model and that calculated by internal standard method (wt%). The solid lines shows the $y = x$ correlation and the dashed lines depict a ± 5 wt% interval.

corresponding with the dehydration of amorphous C-(A)-S-H and xonotlite, respectively. The test results were in good agreement with QXRD results presented in Fig. 12. On the other hand, the non-evaporable water content of all fly ash modified samples showed stable non-evaporable water content, which increased slightly with curing time in the systems containing both fly ash and silica. The non-evaporable water content of fly ash modified slurries ranged

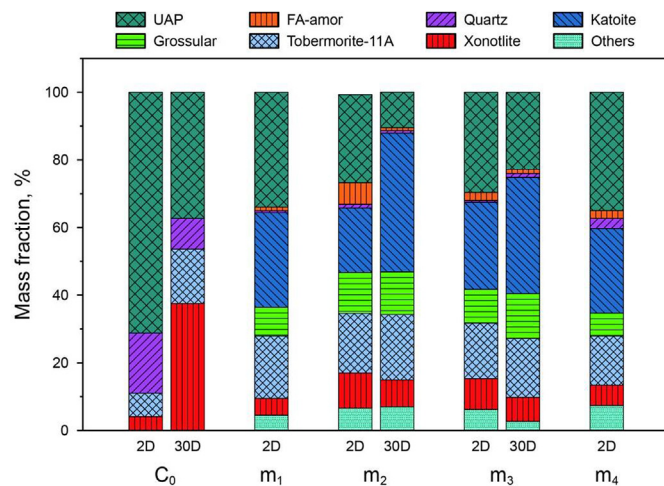


Fig. 9. Phase compositions of unstable systems at various curing time. (“Others” refers to minor phases such as calcium iron silicate hydroxide, grossite, etc.; “UAP” refers to unidentified amorphous phases, which mainly consists of C-(A)-S-H).

from 0.13 to 0.18 g/g dry blend at 30 d, far more than that of control slurry C_0 , suggesting that the addition of fly ash increased the chemically combined water in the hydration products, especially over long-term curing. The derivative curves of fly ash modified slurries showed two main decomposition peaks, one at approximately 210 °C, the other at approximately 420 °C. The first peak corresponds with the dehydration of C-(A)-S-H, while the second peak corresponds with the dehydration of calcium silicoaluminate hydrate such as katoite and grossular (Frías et al., 2022). The second peak in slurries m_1 to m_3 were apparently higher than that in

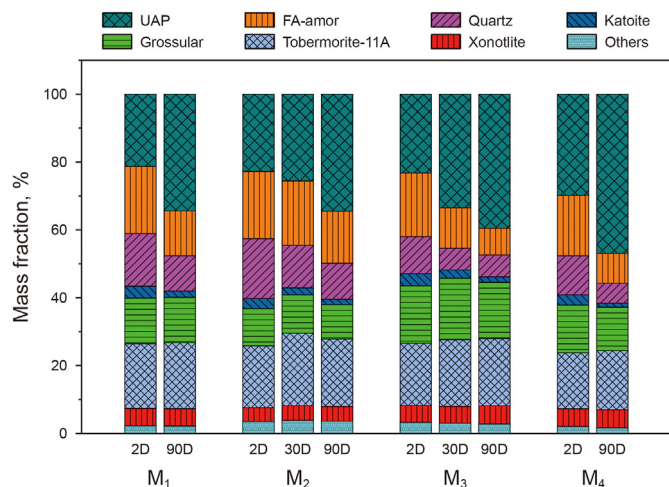


Fig. 10. Phase compositions of stable systems at various curing time. (“Others” refers to minor phases such as calcium iron silicate hydroxide, grossite, etc.; “UAP” refers to unidentified amorphous phases, which mainly consists of C-(A)-S-H).

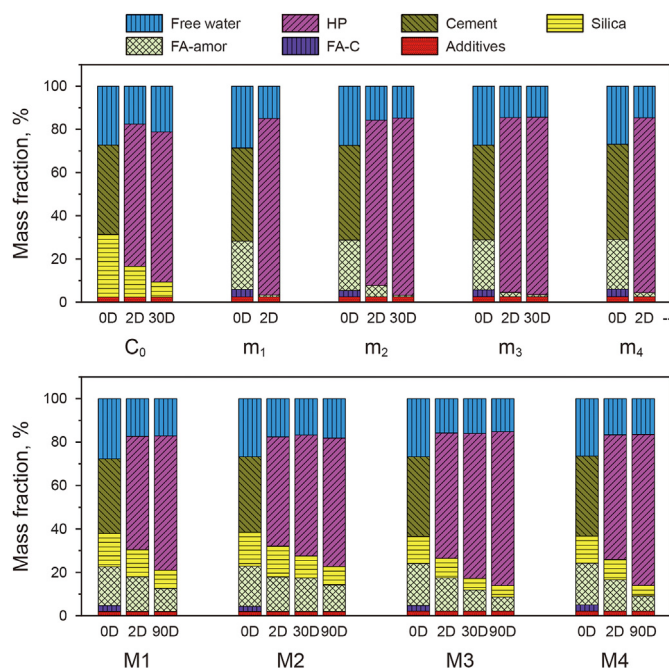


Fig. 11. Composition evolution of different systems at various curing time. (“0 D” is the cement slurry composition before hydration; “HP” refers to all hydration products; “Free water” is evaporable water in set cement; “FA-C” and “FA-amor” refer to crystalline and amorphous components in fly ash, respectively; “additives” are solid components of all additives).

slurries M₁ to M₄, suggesting more kaotite and grossular contents in the former, which is consistent with QXRD test results.

5. Discussion and future work

Cementing high-temperature deep wells presents significantly different challenges compared with steam-injection wells. High-temperature deep wells requires the cement to set and cure in one-step at high temperatures, while steam injection wells require the cement to set at relatively low temperatures and cure at high temperatures. As revealed by several recent studies, the strength retrogression problem for high-temperature deep well conditions

is much more difficult to solve than that for steam injection well conditions. Strategies such as optimizing the particle size and dosage of silica, employment of other admixtures such as alpha-alumina, fiber or nano-graphene reinforcement materials, and highly reactive amorphous silica, all seemed to be ineffective in preventing long-term strength retrogression (Pang et al., 2021; Qin et al., 2023). This study presented a novel method of improving the long-term strength stability of traditional silica-enriched oil well cement by introducing fly ash to the system and achieved excellent test results. The working mechanism of fly ash in preventing long-term strength retrogression is revealed by comprehensive microscopic and phase composition analysis of the set cement. The possible reason that the combined use of fly ash and silica can improve the long-term strength stability of oil well cement systems is twofold: first of all, the xonotlite phase related to poor strength was inhibited; secondly, the stability of C-S-H was improved by introducing aluminum inclusions to form C-(A)-S-H. C-(A)-S-H is known to have better stability and micromechanical properties than C-S-H (Hou, et al., 2015; Zhu et al., 2022). However, the reason that the cement-fly-ash systems (m systems) also experienced strength retrogression may be due to its high Ca/Si ratio (ranging from 1.42 to 1.59). It has been shown that the stability of the C-(A)-S-H with a lower Ca/Si ratio is superior to that of the C-(A)-S-H with a higher Ca/Si ratio due to fewer defects in the silica chain, lower polymerization, and small gel pore volume (Wang et al., 2022). Additionally, only limited number of mixture designs are investigated at one curing temperature here. A more comprehensive investigation of the admixture design parameters, such as the ratio between fly ash and silica and their total dosage, is needed in the future. The effect of different curing temperature on the test results should also be evaluated in future studies.

6. Conclusions

The influences of fly ash and silica on the high temperature resistance of oil well cement (directly set and cured under the condition of 200 °C and 50 MPa for different curing time) were studied experimentally. The following main conclusions can be drawn.

- (1) The addition of silica or fly ash individually in oil well cement cannot prevent the long-term strength retrogression, while their combined addition can not only stabilize the mixture but also result in increases in strength and decreases in permeability of the set cement with increasing curing time. The compressive strength was increased by 11.1%–101%, while the permeability was decreased by 36.2%–79.7% from 2 to 90 d for the four different systems studied.
- (2) The pore size and total porosity of oil well cement systems containing both fly ash and silica were decreased with increasing curing time, suggesting that the combined use of the two admixtures effectively prevented microstructure coarsening of oil well cement systems over long-term curing at HPHT conditions, which is consistent with permeability test results.
- (3) The cement slurries containing only silica showed significant conversion of amorphous C-(A)-S-H to xonotlite during long-term curing while the cement slurries containing only fly ash showed significant conversion of amorphous C-(A)-S-H to kaotite and grossular during long-term curing, which are possibly the cause of strength retrogression of these systems. The cement slurries containing both silica and fly ash exhibited more stable compositions, and the amorphous C-(A)-S-H content increased with time during long-term

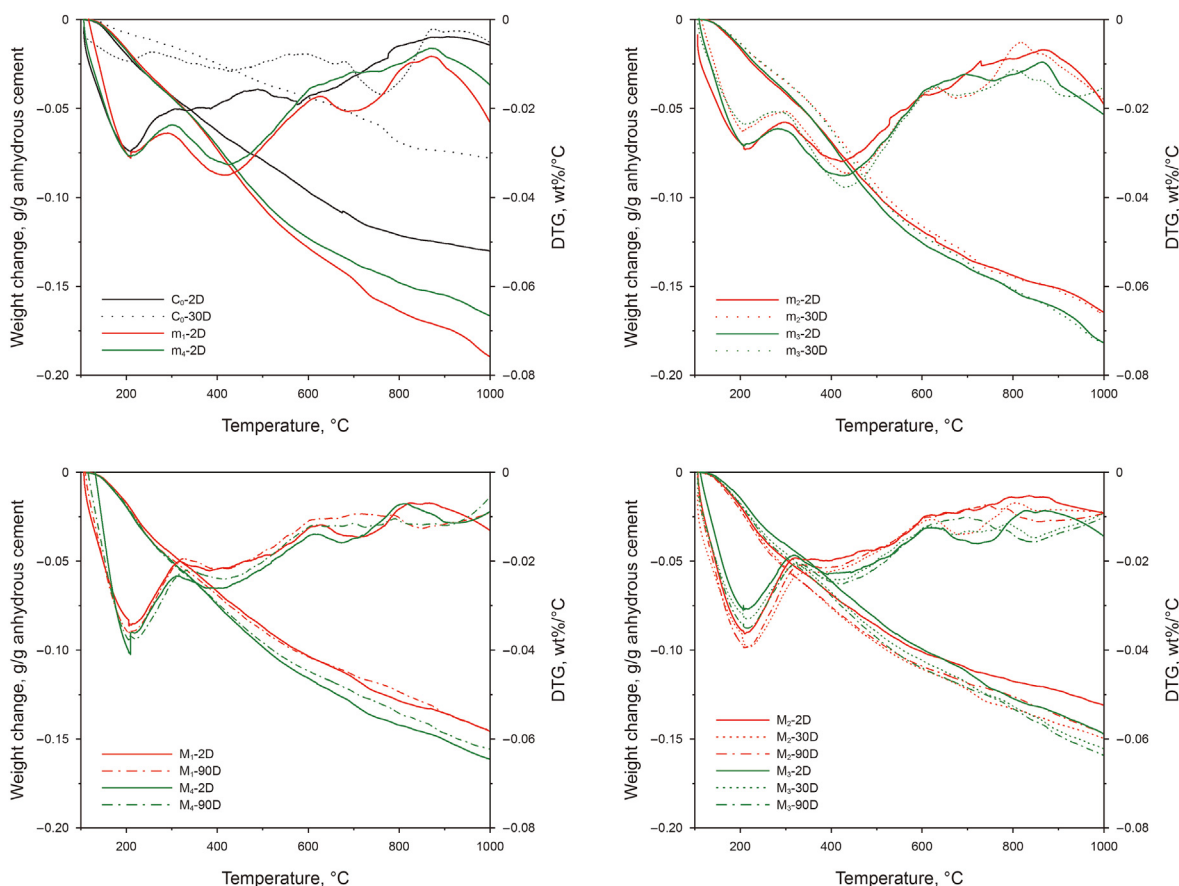


Fig. 12. TGA test results of set cement at various curing time.

curing, which explained the long-term stability of their physical and mechanical properties.

- (4) Within the scope of this study, test results show that the different types of fly ash used had no significant differences in their abilities to prevent the long-term deteriorations of traditional silica-enriched system properties at HPHT conditions.

Declaration of competing interest

The authors declare that they have no known competing financial interests or personal relationships that could have appeared to influence the work reported in this paper.

Acknowledgement

Financial support comes from National Natural Science Foundation of China (No. 51974352 and No. 52288101) as well as from China University of Petroleum (East China) (No. 2018000025 and No. 2019000011).

Appendix A. Supplementary data

Supplementary data to this article can be found online at <https://doi.org/10.1016/j.petsci.2023.09.010>.

References

Adjei, S., Elkhatatny, S., Aggrey, W.N., et al., 2022. Geopolymer as the future oil-well cement: a review. *J. Petrol. Sci. Eng.* 208, 109485. <https://doi.org/10.1016/j.petrol.2021.10K9485>.

- Ahdaya, M., Imqam, A., 2019. Fly ash class C based geopolymer for oil well cementing. *J. Petrol. Sci. Eng.* 179, 750–757. <https://doi.org/10.1016/j.petrol.2019.04.106>.
- Ahmaruzzaman, M., 2010. A review on the utilization of fly ash. *Prog. Energy Combust. Sci.* 36, 327–363. <https://doi.org/10.1016/j.pecs.2009.11.003>.
- Allahviridzadeh, P., 2020. A review on geothermal wells: well integrity issues. *J. Clean. Prod.* 275, 124009. <https://doi.org/10.1016/j.jclepro.2020.124009>.
- Antiohos, S.K., Papadakis, V.G., Chaniotakis, E., Tsimas, S., 2007. Improving the performance of ternary blended cements by mixing different types of fly ashes. *Cement Concr. Res.* 37 (6), 877–885. <https://doi.org/10.1016/j.cemconres.2007.02.017>.
- Bullerjahn, F., Mehringskötter, M., 2021. Synthetic granulated blast furnace-like slag from bauxite residue smelting and its use in multi-component Portland composite cement. *J. Clean. Prod.* 329, 129667. <https://doi.org/10.1016/j.jclepro.2021.129667>.
- Chow, S.Y., Kalousek, G.L., 1976. Research on cements for geothermal and deep oil wells. *Soc. Petrol. Eng. J.* 16, 307–309. <https://doi.org/10.2118/5940-PA>.
- Cho, Y.K., Jung, S.H., Choi, Y.C., 2019. Effects of chemical composition of fly ash on compressive strength of fly ash cement mortar. *Construct. Build. Mater.* 204, 255–264. <https://doi.org/10.1016/j.conbuildmat.2019.01.208>.
- Christidis, G.E., Dimitriadi, M., Triantafyllou, G., et al., 2021. Quantitative analysis of Portland cement clinker with Rietveld refinement: implications of the amorphous matter. *Mater. Proc.* 5 (1), 75. <https://doi.org/10.3390/materproc2021005075>.
- Churakov, S.V., Mandaliev, P., 2008. Structure of the hydrogen bonds and silica defects in the tetrahedral double chain of xonotlite. *Cement Concr. Res.* 38, 300–311. <https://doi.org/10.1016/j.cemconres.2007.09.014>.
- Costa, B.L.D.S., Souza, G.G.D., Freitas, J.C.D.O., et al., 2017. Silica content influence on cement compressive strength in wells subjected to steam injection. *J. Petrol. Ence Eng.* 158, 626–633. <https://doi.org/10.1016/j.petrol.2017.09.006>.
- De Maeijer, P.K., Craeye, B., Snellings, R., et al., 2020. Effect of ultra-fine fly ash on concrete performance and durability. *Construct. Build. Mater.* 263, 120493. <https://doi.org/10.1016/j.conbuildmat.2020.120493>.
- De Matos, P.R., Neto, J.S.A., Sakata, R.D., et al., 2022. Strategies for XRD quantitative phase analysis of ordinary and blended Portland cements. *Cem. Concr. Compos.* 131, 104571. <https://doi.org/10.1016/j.cemconcomp.2022.104571>.
- Frías, M., Martínez-Ramírez, S., de la Villa, R.V., et al., 2022. New scientific evidence of the effect of high temperatures and long curing times on MK-blended

- cement paste mineralogy. *Cement Concr. Res.* 152, 106657. <https://doi.org/10.1016/j.cemconres.2021.106657>.
- Giergiczny, Z., 2019. Fly ash and slag. *Cement Concr. Res.* 124, 105826. <https://doi.org/10.1016/j.cemconres.2019.105826>.
- Guo, Y.C., Shen, A.Q., He, T.Q., et al., 2016. Pore structure research on pavement cement concrete subjected to coupling effect of fatigue load and cyclic freeze-thaw in seasonally frozen ground region. *China J. Highw. Transp.* 29 (8), 29. <http://zggglxb.chd.edu.cn/EN/Y2016/V29/I8/29> (in Chinese).
- Helmi, M., Hall, M.R., Stevens, L.A., et al., 2016. Effects of high-pressure/temperature curing on reactive powder concrete microstructure formation. *Construct. Build. Mater.* 105, 554–562. <https://doi.org/10.1016/j.conbuildmat.2015.12.147>.
- Hemalatha, T., Ramaswamy, A., 2017. A review on fly ash characteristics—Towards promoting high volume utilization in developing sustainable concrete. *J. Clean. Prod.* 147, 546–559. <https://doi.org/10.1016/j.jclepro.2017.01.114>.
- Hemalatha, T., Sasmal, S., 2019. Early-age strength development in fly ash blended cement composites: investigation through chemical activation. *Mag. Concr. Res.* 71, 260–270. <https://doi.org/10.1680/jmacr.17.00336>.
- Hou, D., Li, Z., Zhao, T., 2015. Reactive force field simulation on polymerization and hydrolytic reactions in calcium aluminate silicate hydrate (C-A-S-H) gel: structure, dynamics and mechanical properties. *RSC Adv.* 5, 448–461. <https://doi.org/10.1039/C4RA10645H>.
- Hu, W., Bao, J., Hu, B., 2013. Trend and progress in global oil and gas exploration. *Petrol. Explor. Dev.* 40, 439–443. [https://doi.org/10.1016/S1876-3804\(13\)60055-5](https://doi.org/10.1016/S1876-3804(13)60055-5).
- Iverson, B., Waugh, B., Maxson, J., 2014. High-temperature exposure of oil well cements. *Char. Minerals Metals Mater.* 2014, 17–24.
- Jansen, D., Goetz-Neunhoeffer, F., Lothenbach, B., et al., 2012. The early hydration of Ordinary Portland Cement (OPC): an approach comparing measured heat flow with calculated heat flow from QXRD. *Cement Concr. Res.* 42, 134–138. <https://doi.org/10.1016/j.cemconres.2011.09.001>.
- Jiang, T., Geng, C., Yao, X., Song, W., et al., 2021. Long-term thermal performance of oil well cement modified by silica flour with different particle sizes in HTHP environment. *Construct. Build. Mater.* 296, 123701. <https://doi.org/10.1016/j.conbuildmat.2021.123701>.
- Juenger, M.C.G., Siddique, R., 2015. Recent advances in understanding the role of supplementary cementitious materials in concrete. *Cement Concr. Res.* 78, 71–80. <https://doi.org/10.1016/j.cemconres.2015.03.018>.
- Jupe, A.C., Wilkinson, A.P., Luke, K., et al., 2008. Class H cement hydration at 180 °C and high pressure in the presence of added silica. *Cement Concr. Res.* 38, 660–666. <https://doi.org/10.1016/j.cemconres.2007.12.004>.
- Khalifeh, M., SaasKen, A., Hodne, H., et al., 2018. Geopolymers as an alternative for oil well cementing applications: a review of advantages and concerns. *J. Energy Resour. Technol.* 140, 9. <https://doi.org/10.1115/1.4040192>.
- Krakowiak, K.J., Thomas, J.J., James, S., et al., 2018. Development of silica-enriched cement-based materials with improved aging resistance for application in high-temperature environments. *Cement Concr. Res.* 105, 91–110. <https://doi.org/10.1016/j.cemconres.2018.01.004>.
- Krakowiak, K.J., Thomas, J.J., Musso, S., et al., 2015. Nano-chemo-mechanical signature of conventional oil-well cement systems: effects of elevated temperature and curing time. *Cement Concr. Res.* 67, 103–121. <https://doi.org/10.1016/j.cemconres.2014.08.008>.
- Lam, L., Wong, Y.L., Poon, C.S., 2000. Degree of hydration and gel/space ratio of high-volume fly ash/cement systems. *Cement Concr. Res.* 30 (5), 747–756. [https://doi.org/10.1016/S0008-8846\(00\)00213-1](https://doi.org/10.1016/S0008-8846(00)00213-1).
- Le Saoût, G., Kocaba, V., Scrivener, K., 2011. Application of the Rietveld method to the analysis of anhydrous cement. *Cement Concr. Res.* 41, 133–148. [doi:10.1016/j.cemconres.2010.10.003](https://doi.org/10.1016/j.cemconres.2010.10.003).
- Li, N., Pang, X., Ai, Z., et al., 2020. Composition optimization and strength decline mechanism of oil well cement slurry at 200 °C. *J. Chin. Ceram. Soc.* 48 (11), 1824–1833. <https://doi.org/10.14062/j.jissn.0454-5648.20200300> (in Chinese).
- Li, Q., Zhao, Y., Chen, H., et al., 2021. Effect of waste corn stalk ash on the early-age strength development of fly ash/cement composite. *Construct. Build. Mater.* 303, 124463. <https://doi.org/10.1016/j.conbuildmat.2021.124463>.
- Liu, H., Bu, Y., Zhou, A., Du, J., Zhou, L., Pang, X., 2021. Silica sand enhanced cement mortar for cementing steam injection well up to 380 °C. *Construct. Build. Mater.* 308, 125142. <https://doi.org/10.1016/j.conbuildmat.2021.125142>.
- Liu, H., Qin, J., Zhou, B., et al., 2022. Effects of curing pressure on the long-term strength retrogression of oil well cement cured under 200 °C. *Energies* 15, 6071. <https://doi.org/10.3390/en15166071>.
- Ma, B., Li, H., Li, X., et al., 2016. Influence of nano-TiO₂ on physical and hydration characteristics of fly ash–cement systems. *Construct. Build. Mater.* 122, 242–253. <https://doi.org/10.1016/j.conbuildmat.2016.02.087>.
- Mejdi, M., Wilson, W., Saillio, M., et al., 2022. Hydration and microstructure of glass powder cement pastes—A multi-technique investigation. *Cement Concr. Res.* 151, 106610. <https://doi.org/10.1016/j.cemconres.2021.106610>.
- Meng, T., Yu, Y., Wang, Z., 2017. Effect of nano-CaCO₃ slurry on the mechanical properties and micro-structure of concrete with and without fly ash. *Compos. B Eng.* 117, 124–129. <https://doi.org/10.1016/j.compositesb.2017.02.030>.
- Naber, C., Stegmeyer, S., Jansen, D., et al., 2019. The PONKCS method applied for time resolved XRD quantification of supplementary cementitious material reactivity in hydrating mixtures with ordinary Portland cement. *Construct. Build. Mater.* 214, 449–457. <https://doi.org/10.1016/j.conbuildmat.2019.04.157>.
- Paiva, M., Silva, E., Melo, D., et al., 2018. A geopolymer cementing system for oil wells subject to steam injection. *J. Petrol. Sci. Eng.* 169, 748–759. <https://doi.org/10.1016/j.petrol.2018.06.022>.
- Pang, X., Qin, J., Sun, L., et al., 2021. Long-term strength retrogression of silica-enriched oil well cement: a comprehensive multi-approach analysis. *Cement Concr. Res.* 144, 106424. <https://doi.org/10.1016/j.cemconres.2021.106424>.
- Pang, X., Sun, L., Chen, M., et al., 2022. Influence of curing temperature on the hydration and strength development of Class G Portland cement. *Cement Concr. Res.* 156, 106776. <https://doi.org/10.1016/j.cemconres.2022.106776>.
- Pernites, R.B., Santra, A.K., 2016. Portland cement solutions for ultra-high temperature wellbore applications. *Cem. Concr. Compos.* 72, 89–103. <https://doi.org/10.1016/j.cemconcomp.2016.05.018>.
- Polavaram, K.C., Garg, N., 2021. Enabling phase quantification of anhydrous cements via Raman imaging. *Cement Concr. Res.* 150, 106592. <https://doi.org/10.1016/j.cemconres.2021.106592>.
- Pu, L., Xu, P., Xu, M., et al., 2022. Lost circulation materials for deep and ultra-deep wells: A review. *J. Petrol. Sci. Eng.* 110404. <https://doi.org/10.1016/j.petrol.2022.110404>.
- Qin, J., Pang, X., Cheng, G., et al., 2021. Influences of different admixtures on the properties of oil well cement systems at HPTH conditions. *Cem. Concr. Compos.* 123, 104202. <https://doi.org/10.1016/j.cemconcomp.2021.104202>.
- Qin, J., Pang, X., Li, H., et al., 2022. Mechanism of long-term strength retrogression of silica-enriched Portland cement assessed by quantitative X-ray diffraction analysis. *Front. Mater.* 9, 982192. <https://doi.org/10.3389/fmats.2022.982192>.
- Qin, J., Pang, X., Santra, A.K., et al., 2023. Various admixtures to mitigate the long-term strength retrogression of Portland cement cured under high pressure and high temperature conditions. *J. Rock Mech. Geotech. Eng.* 15 (1), 191–203. <https://doi.org/10.1016/j.jrmge.2022.02.005>.
- Reddy, B., Zhang, J., Ellis, M., 2016. Cement strength retrogression issues in offshore deep water applications—do we know enough for safe cementing?. In: *Offshore Technology Conference, OnePetro*. <https://doi.org/10.4043/27012-MS>.
- Salehi, S., Khattak, J., Saleh, F.K., et al., 2019. Investigation of mix design and properties of geopolymers for application as wellbore cement. *J. Petrol. Sci. Eng.* 178, 133–139. <https://doi.org/10.1016/j.petrol.2019.03.031>.
- Salim, P., Amani, M., 2013. Principal points in cementing geothermal wells. *Adv. Petrol. Explor. Dev.* 5 (1), 77–91. <https://doi.org/10.3968/j.aped.1925543820130501.1145>.
- Scarlett, N.V.Y., Madsen, I.C., 2006. Quantification of phases with partial or no known crystal structures. *Powder Diffr.* 21, 278–284. <https://doi.org/10.1154/1.2362855>.
- Scrivener, K., Füllmann, T., Gallucci, E., et al., 2004. Quantitative study of Portland cement hydration by X-ray diffraction/Rietveld analysis and independent methods. *Cement Concr. Res.* 34, 1541–1547. <https://doi.org/10.1016/j.cemconres.2004.04.014>.
- Scrivener, K., Snellings, R., Lothenbach, B., 2016. *A Practical Guide to Microstructural Analysis of Cementitious Materials*. Crc Press Boca Raton, FL, USA.
- Shaw, S., Clark, S.M., Henderson, C.M.B., 2000. Hydrothermal formation of the calcium silicate hydrates, tobermorite (Ca₅Si₆O₁₆(OH)₂·4H₂O) and xonotlite (Ca₆Si₆O₁₇(OH)₂): an in situ synchrotron study. *Chem. Geol.* 167, 129–140. [https://doi.org/10.1016/S0009-2541\(99\)00205-3](https://doi.org/10.1016/S0009-2541(99)00205-3).
- Shen, A., Lin, S., Guo, Y., et al., 2018. Relationship between flexural strength and pore structure of pavement concrete under fatigue loads and Freeze-thaw interaction in seasonal frozen regions. *Construct. Build. Mater.* 174, 684–692. <https://doi.org/10.1016/j.conbuildmat.2018.04>.
- Shen, P., Lu, L., He, Y., et al., 2019. The effect of curing regimes on the mechanical properties, nano-mechanical properties and microstructure of ultra-high performance concrete. *Cement Concr. Res.* 118, 1–13. <https://doi.org/10.1016/j.cemconres.2019.01.004>.
- Snellings, R., Salze, A., Scrivener, K.L., 2014. Use of X-ray diffraction to quantify amorphous supplementary cementitious materials in anhydrous and hydrated blended cements. *Cement Concr. Res.* 64, 89–98. <https://doi.org/10.1016/j.cemconres.2014.06.011>.
- Soin, A.V., Catalan, L.J., Kinrade, S.D., 2013. A combined QXRD/TG method to quantify the phase composition of hydrated oil well cements. *Cement Concr. Res.* 48, 17–24. <https://doi.org/10.1016/j.cemconres.2013.02.007>.
- Stetsko, Y.P., Shanahan, N., Deford, H., et al., 2017. Quantification of supplementary cementitious content in blended Portland cement using an iterative Rietveld–PONKCS technique. *J. Appl. Crystallogr.* 50, 498–507. <https://doi.org/10.1107/S1600576717002965>.
- Sun, Z., Vollpracht, A., 2018. Isothermal calorimetry and in-situ XRD study of the NaOH activated fly ash, metakaolin and slag. *Cement Concr. Res.* 103, 110–122. <https://doi.org/10.1016/j.cemconres.2017.10.004>.
- Swayze, M., 1954. Effect of high temperature on strength of oil-well cements (Mid-continent district study committee on cementing practices and testing of oil-well cements). *Vacuum* 13 (7–8), 206. [https://doi.org/10.1016/0042-207X\(63\)90451-2](https://doi.org/10.1016/0042-207X(63)90451-2).
- Wang, H., Ge, Y., Shi, L., 2017. Technologies in deep and ultra-deep well drilling: present status, challenges and future trend in the 13th Five-Year Plan period (2016–2020). *Nat. Gas. Ind. B* 4, 319–326. <https://doi.org/10.1016/j.ngib.2017.09.001>.
- Wang, J., Huang, T., Cheng, G., et al., 2019. Effects of fly ash on the properties and microstructure of alkali-activated FA/BFS repairing mortar. *Fuel* 256, 115919. <https://doi.org/10.1016/j.fuel.2019.115919>.
- Wang, J., Hu, Z., Chen, Y., et al., 2022. Effect of Ca/Si and Al/Si on micromechanical properties of C-(A)-SH. *Cement Concr. Res.* 157, 106811. <https://doi.org/10.1016/j.cemconres.2022.106811>.
- Wei, Y., Yao, W., Xing, X., et al., 2012. Quantitative evaluation of hydrated cement modified by silica fume using QXRD, 27Al MAS NMR, TG–DSC and selective

- dissolution techniques. *Construct. Build. Mater.* 36, 925–932. <https://doi.org/10.1016/j.conbuildmat.2012.06.075>.
- Wolf, J.J., Jansen, D., Goetz-Neunhoeffler, F., et al., 2019. Mechanisms of early ettringite formation in ternary CSA–OPC–anhydrite systems. *Adv. Cement Res.* 31, 195–204. <https://doi.org/10.1680/jadcr.18.00115>.
- Wolf, J.J., Jansen, D., Goetz-Neunhoeffler, F., et al., 2020. Application of thermodynamic modeling to predict the stable hydrate phase assemblages in ternary CSA-OPC-anhydrite systems and quantitative verification by QXRD. *Cement Concr. Res.* 128, 105956. <https://doi.org/10.1016/j.cemconres.2019.105956>.
- Yildirim, K., Sümer, M., 2013. Effects of sodium chloride and magnesium sulfate concentration on the durability of cement mortar with and without fly ash. *Compos. B Eng.* 52, 56–61. <https://doi.org/10.1016/j.compositesb.2013.03.040>.
- Zhou, C., Ren, F., Wang, Z., et al., 2017. Why permeability to water is anomalously lower than that to many other fluids for cement-based material? *Cement Concr. Res.* 100, 373–384. <https://doi.org/10.1016/j.cemconres.2017.08.002>.
- Zhu, X., Ren, Q., He, B., et al., 2022. Upscaling degradation of cementitious calcium (aluminate) silicate hydrate upon ultra-low temperature attack: a multiscale insight and a bottom-up enhancement route. *Compos. B Eng.* 243, 110122. <https://doi.org/10.1016/j.compositesb.2022.110122>.